Thin Solid Films 535 (2013) 311–313

Contents lists available at SciVerse ScienceDirect

Thin Solid Films

journal homepage: www.elsevier.com/locate/tsf

Born effective charges of Cu_2ZnSnS_4 quaternary compound: First principles calculations

T.A. Oliveira, J. Coutinho *, V.J.B. Torres

Department of Physics & I3N, University of Aveiro, Campus Santiago, 3810-193 Aveiro, Portugal

ARTICLE INFO

Available online 15 November 2012

Keywords:
Photovoltaics
CZTS
Born effective charge
Transverse charge

ABSTRACT

Toxicity and scarceness stand as major handicaps for $CuInGaSe_2$ and $CuInGaS_2$ based compounds when applied as photoactive layers in solar cells. As a result, quaternary semiconductors Cu_2ZnSnS_4 and $Cu_2ZnSnSe_4$ are emerging as serious contenders to take their place. We report on the structural and dynamical properties of Cu_2ZnSnS_4 by using first principles plane-wave pseudopotential calculations. The most stable kesterite and stannite structures were considered and the Born effective charge (transverse charge) tensors were obtained by using self-consistent finite-electric field calculations within the Berry phase approach. These quantities may allow us to understand longitudinal and transverse optical splittings from vibrational spectra of this class of materials and related alloys.

1. Introduction

Meeting the increasing demand for cleaner and cheaper energy sources has recently lead to unprecedented research efforts on photovoltaic (PV) solar-energy conversion. While silicon-based solar cells dominate the PV market with large-scale facilities approaching the 1.0 $/Wp cost threshold, the main focus of the current research in second generation photovoltaics is to develop cheaper materials/processes without compromising power conversion efficiencies (PCE). In this field, quaternary alloys such as $Cu_2In_{1-x}Ga_xSe_2$ (CIGS), have drawn much attention as promising photoactive layer candidates in solar cell devices, with reported PCE values of up to 20% [1]. However, increasing environmental concerns as well as expected restrictions in the supply of In and other rare elements have led to the search for alternative chalcopyrite-like materials.

Quaternary semiconductors Cu_2ZnSnS_4 (CZTS) and $Cu_2ZnSnSe_4$ (CZTSe) are emerging as a serious contenders to replace CIGS since all its elements are abundant and non-toxic. The direct band-gap energy of $E_g \approx 1.4-1.6$ eV [2–6] and the high optical absorption coefficient (10^{-4} cm^{-1}) [4,5] make them suitable for photovoltaics. CZTS- and CZTSe-based solar cells have been reported to reach PCE values of 6.7% and 3.2%, respectively [7,8], and this was recently improved to 9.7% by using $Cu_2ZnSn(S_{1-x}Se_x)_4$ photoactive alloys [9]. These encouraging results have prompted interest for a better understanding of the properties of CZTS, CZTSe and corresponding alloys, both through experimental and theoretical means.

It has been shown, both experimentally [3–5] and theoretically [10], that CZTS and CZTSe have two particularly stable crystalline structures at room temperature, namely kesterite (space group S_4^2 and referred as KS) and stannite (space group D_{2d}^{11} and referred as ST). Their respective conventional cells are depicted in Fig. 1(a) and (b). Besides phase stability, other theoretical investigations have dealt with properties such as native defect formation [11,12], electronic band structure [10,13–15], carrier transport [16] and optical properties [15]. Despite these advances, relatively little has been done about understanding dynamical properties. There are some infra-red [17] and Raman experiments [18–23], but first-principles reports regarding these properties are even fewer [24,25]. First-principles vibrational spectrum for CZTSe using the finite-displacement method [24], pointed out some noticeable differences between KS and ST phase data which could be well used for structural identification. However, in a broader analysis towards calculating the dynamical properties of $CZTS_xSe_{1-x}$ alloys, one needs to determine accurately the dynamical charges of individual ions.

The Born effective charge (also known as transverse charge) $\mathbf{Z}^*$ is directly related to the change in the polarization created by atomic displacement. This change in polarization is a quantity that can be experimentally measured, and therefore may be used to characterize the atomic and electronic nature of matter. The Born effective charge is used to quantify the long-range Coulomb interaction responsible for the splitting between transverse and longitudinal optical phonon modes [26], and likewise, its knowledge may turn out to be decisive to understand optical spectra of CZTS (here taken as prototypical) and materials alike. This is particularly relevant in providing insight for the characterization and improvement of CZTS polycrystalline thin films, where several crystalline structures, derived phases and stoichiometric

* Corresponding author.
E-mail address: jose.coutinho@ua.pt (J. Coutinho).

0040-6090/$ – see front matter © 2012 Elsevier B.V. All rights reserved.
http://dx.doi.org/10.1016/j.tsf.2012.10.115

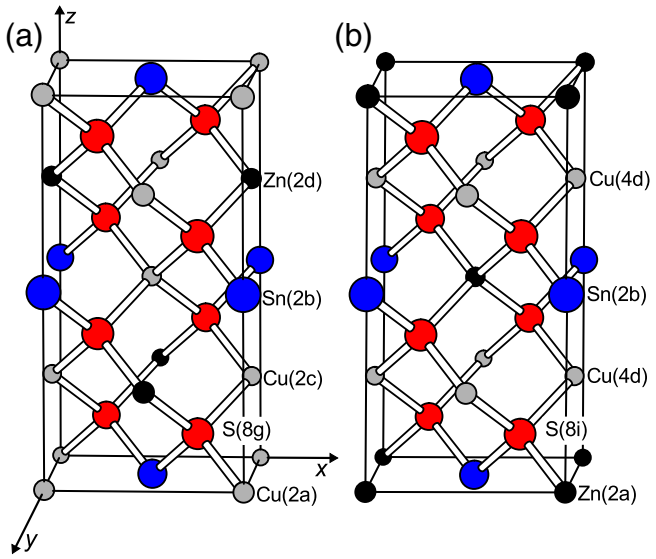

Fig. 1. Crystalline structure of (a) kesterite and (b) stannite conventional cells of CZTS. Cu, Zn, Sn and S species are shown in gray, black, blue and red, respectively. Wyckoff positions are also represented on each species.

defects occur. Since $\mathbf{Z}^*$ is sensitive to the structural properties of the material [27], results for both phase structures of CZTS are reported independently.

2. Method

Density functional theory calculations as implemented in the ABINIT code [28] were performed along with the local density approximation (LDA) to the exchange correlation potential [29]. Explicit treatment of core electrons was avoided by using the norm-conserving pseudopotentials by Hartwigsen, Goedecker and Hutter [30]. The valence structure of Cu, Zn, Sn and S individual atoms was $3d^{10}4s^1$, $3d^{10}4s^2$, $5s^25p^2$ and $3s^23p^4$, respectively. Wave functions were expanded in plane waves with a kinetic energy up to a cut-off $E_{\mathrm{cut}=150}$ Ha, and the electron density and potential terms were dealt in reciprocal space by fast Fourier transformation.

The Brillouin zone for both KS and ST structures was sampled with the help of a Γ-centered $8\times8\times8$ symmetry-folded special **k**-point mesh, according to the recipe by Monkhorst and Pack [31]. The convergence of E_{cut} and **k**-point sampling was independently and systematically evaluated, until the total energy change was less than 10^{-4} Ha. For each structure, lattice vectors and atomic positions were allowed to relax (although enforcing the symmetry of the system) using an adaptation of the Broyden–Fletcher–Goldfarb–Shanno minimization method [32]. This was carried out until all atomic forces became smaller than a tolerance of 2.6 meV/Å. Finally, from inspection of each atom site and symmetry reduction, we found all irreducible tensor coordinates which were determined by self-consistent finite-electric field calculations within the Berry phase approach [33].

Fig. 1 depicts both KS and ST conventional unit-cell structures of CZTS. The KS structure with space group S_4^2 ($I\bar{4}$; no. 82) has in its primitive unit cell two Cu atoms at Wyckoff positions *2a* and *2c*, one Zn atom at a site of type *2d*, one Sn atom at a site *2b* and four S atoms at *8g* sites. All these positions have S_4 site symmetry, except the sulfur site that has C_1 (close to C_{1h}) site symmetry. The ST structure with space group D_{2d}^{11} ($I\bar{4}2m$; no. 121) has two equivalent Cu atoms at *4d* Wyckoff positions (S_4 site symmetry), one Zn and one Sn atoms at *2a* and *2b* sites, respectively (both with D_{2d} site symmetry) and four S atoms at *8i* sites with C_{1h} site symmetry. It is worth noting that properly relaxed and well-optimized structural parameters are essential for finite electric field calculations.

2.1. Finite electric field response

The Born effective charge elements $Z^*_{\kappa,\alpha\beta}$ of species κ are proportional to the change in the macroscopic polarization $\mathcal{P}_\beta$ along the direction β, that results from the collective nuclear displacement $\tau_{\kappa\alpha}$ of the atomic sub-lattice κ along direction α,

$$Z^*_{\kappa,\alpha\beta} = \Omega_0 \frac{\partial \mathcal{P}_\beta}{\partial \tau_{\kappa\alpha}}\bigg|_{\mathcal{E}=0} = \frac{\partial F_{\kappa,\alpha}}{\partial \mathcal{E}_\beta}\bigg|_{\tau_{\kappa\alpha}=0}, \quad (1)$$

where Ω_0 is the unit cell volume and the result is obtained under conditions of zero macroscopic electric field ($\mathcal{E}=0$) [34]. Alternatively, $\mathbf{Z}^*$ can be obtained from the derivative of the force $F_{\kappa,\alpha}$ along α induced on a sub-lattice κ by a homogeneous effective electric field $\mathcal{E}_\beta$ along β (at the limit of zero atomic displacement) [33]. For finite electric field calculations, atomic forces were obtained for a total of five values of $\mathcal{E}$ around the zero-field with small increments ($\sim 5\times10^{-4}$ V/Å) along all three Cartesian axis. A Born effective charge tensor for each atom is then constructed from the linear fit of the expression $F_{\kappa,\alpha} = Z^*_{\kappa,\alpha\beta}\,\mathcal{E}_\beta$ to the data. Special care was taken to avoid the applied field exceeding the critical field for Zener breakthrough [33], and the self-consistency convergence stop criteria was kept at 3×10^{-9} eV.

3. Results

The calculated lattice parameters a and c for KS and ST structures, along with respective tetragonality ratios $\eta = c/2a$ (see Table 1) confirm the small (almost vanishing) departure from the perfect cubic ratio as reported previously [15,25]. Bulk moduli B and respective pressure derivatives B' have been determined by fitting the calculated data to the Murnaghan equation of state [35], and both figures are in agreement with previous LDA calculations [36,25]. Sulfur anions in kesterite (and stannite) show a small deviation (x, y, z) [and (x, x, z)] from the perfect tetrahedral site, where x, y and z are of the order of 0.1 Å.

The calculated effective charges for both phases are reported in Table 2. It is instructive to put these figures into perspective by comparing the results with those obtained for zincblende and chalopyrite crystals. In Ref. [37] the calculated diagonal elements of the effective charge tensor for copper in $CuInS_2$ were around 1.04–1.10. As show in Table 2, the diagonal elements of the Cu charge tensor in KS are relatively lower, suggesting a higher polarization and electron transfer from Cu to S in CIS. The off-diagonal elements arise from a departure of the local environment from the perfect tetrahedral symmetry. This is especially notorious for the case of the anion atoms that are considerably displaced from the tetrahedral sites, as well as for the case of Cu sites of type *2a* in KS where this deviation is rather small.

Effective charges of Zn in ZnSe and ZnS are known to be about 2 [38], and our calculations are consistent with these figures. While in KS the sulfur first neighbors of Zn occupy a low-symmetry triclinic site, in ST they lie at monoclinic sites. This leads to the small off-diagonal elements of $|Z^*_{\mathrm{Zn},xy}| \sim 0.3$ for the Zn species. There are some similarities between the Sn effective charge tensor elements in the KS and ST structures. In both cases the Sn species lies on *2b* Wyckoff sites, they are directly bonded to the anions, and differ only by its second neighbors. Here the diagonal elements of both phases are rather close, and again, the small off-diagonal components in KS are related to the low site symmetry of the anion sub-lattice.

Table 1
Calculated crystalline parameters (a and c in Å), tetragonality ratio (η), bulk modulus (B in GPa) and its pressure derivative (B') for kesterite and stannite structures of CZTS.

	a	c	η	B	B'
KS	5.322	10.645	1.000	86.8	4.7
ST	5.318	10.659	1.002	86.9	4.7

Table 2
Born effective charges in Cartesian coordinates for kesterite and stannite structures of CZTS. All anions lie on equivalent Wyckoff sites (*8g* and *8i* for kesterite and stannite, respectively) so that $\mathbf{Z}^*_S$ values refer to the position (*x*,*y*,*z*) in kesterite and position (*x*,*x*,*z*) in stannite. Cu related effective charges for kesterite correspond to atom sites (0,0,0) and (0, 1/2, 1/4) of type *2a* and *2c*, respectively. In stannite, both Cu atoms are located at *4d* sites so that only the tensor for Cu atom at position (0, 1/2, 1/4) is reported.

	KS	ST
$\mathbf{Z}^*_{Cu}$	$\begin{pmatrix} 0.65 & 0.08 & \\ -0.08 & 0.65 & \\ & & 0.88 \end{pmatrix}$	
	$\begin{pmatrix} 0.76 & -0.33 & \\ 0.33 & 0.76 & \\ & & 0.70 \end{pmatrix}$	$\begin{pmatrix} 0.89 & -0.31 & \\ 0.31 & 0.89 & \\ & & 0.61 \end{pmatrix}$
$\mathbf{Z}^*_{Zn}$	$\begin{pmatrix} 1.97 & -0.29 & \\ 0.29 & 1.97 & \\ & & 2.14 \end{pmatrix}$	$\begin{pmatrix} 2.19 & & \\ & 2.19 & \\ & & 1.77 \end{pmatrix}$
$\mathbf{Z}^*_{Sn}$	$\begin{pmatrix} 3.16 & -0.05 & \\ 0.05 & 3.16 & \\ & & 3.22 \end{pmatrix}$	$\begin{pmatrix} 3.13 & & \\ & 3.13 & \\ & & 3.10 \end{pmatrix}$
$\mathbf{Z}^*_{S}$	$\begin{pmatrix} -1.81 & -0.06 & -0.78 \\ -0.35 & -1.46 & -0.13 \\ -0.72 & 0.05 & -1.74 \end{pmatrix}$	$\begin{pmatrix} -1.78 & -0.78 & 0.05 \\ -0.78 & -1.78 & 0.05 \\ -0.22 & -0.22 & -1.52 \end{pmatrix}$

Regarding the S effective charge tensor, previous calculations for chalcopyrite-related materials [37] obtained diagonal elements around −2, and are therefore in line with our results.

4. Conclusions

We carried out ab initio density functional calculations of the structural properties and Born effective charge tensors of CZTS in kesterite and stannite phases by a linear-response method. The calculated structural and elastic parameters are in agreement with previous calculations and experiments. All independent Born effective charge tensor elements are reported and they are within the expected magnitude. This report results from a preliminary stage of a wider effort to study the dynamical properties CZTS, CZTSe and CZT(S,Se) alloys, as well as to understand the LO/TO splittings observed in Raman spectra.

Acknowledgments

This work was supported by Fundação para a Ciência e a Tecnologia, Portugal (FCT) under the grants PTDC/CTM-MET/113486/2009 and PEst-C/CTM/LA0025/2011.

References

[1] I. Repins, M.A. Contreras, B. Egaas, C. DeHart, J. Scharf, C.L. Perkins, B. To, R. Noufi, Prog. Photovolt. Res. Appl. 16 (2008) 235.
[2] H. Matsushita, T. Maeda, A. Katsui, T. Takizawa, J. Cryst. Growth 208 (2000) 416.
[3] H. Katagiri, K. Saitoh, T. Washio, H. Shinohara, T. Kurumadani, S. Miyajima, Sol. Energy Mater. Sol. Cells 65 (2001) 141.
[4] J.-S. Seol, S.-Y. Lee, J.-C. Lee, H.-D. Nam, K.-H. Kim, Sol. Energy Mater. Sol. Cells 75 (2003) 155.
[5] T. Tanaka, T. Nagatomo, D. Kawasaki, M. Nishio, Q. Guo, A. Wakahara, A. Yoshida, H. Ogawa, J. Phys. Chem. Solids 66 (2005) 1978.
[6] G.S. Babu, Y.B.K. Kumar, P.U. Bhaskar, V.S. Raja, Semicond. Sci. Technol. 23 (2008) 085023.
[7] H. Katagiri, K. Jimbo, S. Yamada, T. Kamimura, W.S. Maw, T. Fukano, T. Ito, T. Motohiro, Appl. Phys. Express 1 (2008) 041201.
[8] G. Zoppi, I. Forbes, R.W. Miles, P.J. Dale, J.J. Scragg, L.M. Peter, Prog. Photovolt. Res. Appl. 17 (2009) 315.
[9] T.K. Todorov, K.B. Reuter, D.B. Mitzi, Adv. Mater. 22 (2010) E156.
[10] S. Chen, X.G. Gong, A. Walsh, S.-H. Wei, Appl. Phys. Lett. 94 (2009) 041903.
[11] A. Nagoya, R. Asahi, R. Wahl, G. Kresse, Phys. Rev. B 81 (2010) 113202.
[12] S. Chen, X.G. Gong, A. Walsh, S.-H. Wei, Appl. Phys. Lett. 96 (2010) 021902.
[13] S. Nakamura, T. Maeda, T. Wada, Phys. Status Solidi C 6 (2009) 1261.
[14] K. Biswas, S. Lany, A. Zunger, Appl. Phys. Lett. 96 (2010) 201902.
[15] C. Persson, J. Appl. Phys. 107 (2010) 053710.
[16] C. Sevik, T. Çağin, Phys. Rev. B 82 (2010) 045202.
[17] M. Himmrich, H. Haeuseler, Spectrochim. Acta A 47 (1991) 933.
[18] P. Fernandes, P. Salomé, A. da Cunha, Thin Solid Films 517 (2009) 2519.
[19] P. Salomé, P. Fernandes, A. da Cunha, Thin Solid Films 517 (2009) 2531.
[20] M. Altosaar, J. Raudoja, K. Timmo, M. Danilson, M. Grossberg, J. Krustok, E. Mellikov, Phys. Status Solidi A 205 (2008) 167.
[21] M. Grossberg, J. Krustok, K. Timmo, M. Altosaar, Thin Solid Films 517 (2009) 2489.
[22] K. Wang, O. Gunawan, T. Todorov, B. Shin, S.J. Chey, N.A. Bojarczuk, D. Mitzi, S. Guha, Appl. Phys. Lett. 97 (2010) 143508.
[23] H. Yoo, J. Kim, Thin Solid Films 518 (2010) 6567.
[24] N.B.M. Amiri, A. Postnikov, Phys. Rev. B 82 (2010) 205204.
[25] T. Gürel, C. Sevik, T. Çağin, Phys. Rev. B 84 (2011) 205201.
[26] M. Born, K. Huang, Dynamical Theory of Crystal Lattices, Oxford University Press, 1968.
[27] P. Ghosez, J.-P. Michenaud, X. Gonze, Phys. Rev. B 58 (1998) 6224.
[28] X. Gonze, B. Amadon, P.-M. Anglade, J.-M. Beuken, F. Bottin, P. Boulanger, F. Bruneval, D. Caliste, R. Caracas, M. Ct, T. Deutsch, L. Genovese, P. Ghosez, M. Giantomassi, S. Goedecker, D. Hamann, P. Hermet, F. Jollet, G. Jomard, S. Leroux, M. Mancini, S. Mazevet, M. Oliveira, G. Onida, Y. Pouillon, T. Rangel, G.-M. Rignanese, D. Sangalli, R. Shaltaf, M. Torrent, M. Verstraete, G. Zerah, J. Zwanziger, Comput. Phys. Commun. 180 (2009) 2582.
[29] S. Goedecker, M. Teter, J. Hutter, Phys. Rev. B 54 (1996) 1703.
[30] C. Hartwigsen, S. Goedecker, J. Hutter, Phys. Rev. B 58 (1998) 3641.
[31] H.J. Monkhorst, J.D. Pack, Phys. Rev. B 13 (1976) 5188.
[32] H.B. Schlegel, J. Comput. Chem. 3 (1982) 214.
[33] P. Ghosez, J. Junquera, in: First-Principles Modeling of Ferroelectric Oxides Nanostructures, vol. 4, American Scientific Publishers, 2006.
[34] P. Ghosez, X. Gonze, J. Phys. Condens. Matter 12 (2000) 9179.
[35] F.D. Murnaghan, Proc. Natl. Acad. Sci. 30 (9) (1944) 244.
[36] C. Sevik, T. Çağin, Appl. Phys. Lett. 95 (2009) 112105.
[37] J. Łażewski, P.T. Jochym, K. Parlinski, J. Chem. Phys. 117 (2002) 2726.
[38] Y. Yu, J. Zhou, H. Han, C. Zhang, T. Cai, C. Song, T. Gao, J. Alloys Compd. 471 (2009) 492.